Carbon Trends 9 (2022) 100205

Contents lists available at ScienceDirect

Carbon Trends

journal homepage: www.elsevier.com/locate/cartre

Developed performance of rGO/p-Si Schottky junction solar cells

Ahmed M. Suhail[a,b,*], Mazin Ahmed Abed[b], Samer Mahmmod Ahmed[b], Israa M.S. Al-Kadmy[c], Hiyam Altaii[d], Genhua Pan[a]

[a] Wolfson Nanomaterials and Devices Laboratory, School of Engineering, Computing and Mathematics, University of Plymouth, Devon, PL4 8AA, UK
[b] Department of Physics, College of Science, University of Mosul, Mosul, Iraq
[c] Branch of Biotechnology, Department of Biology, College of Science, Mustansiriyah University, Baghdad, Iraq
[d] Department of Biology, College of Science, University of Mosul, Mosul, Iraq

ARTICLE INFO

Article history:
Received 20 July 2022
Revised 10 August 2022
Accepted 22 August 2022

KEYWORDS:
Reduced graphene oxide
Schottky junction solar cell
n-doping
Stability
Efficiency

ABSTRACT

Graphene in combination with Si has been extensively used to prepare efficient and stable p-graphene/n-Si Schottky junction solar cells. In contrast, there is a difficulty in including graphene within the fabrication process of efficient and stable n-graphene/p-Si Schottky junction solar cells. The reason for this is that there is a challenge in achieving an effective and stable n-doping process for graphene or rGO due to the ambient environment. In this work, a novel approach is introduced for preparing more efficient, stable, larger and simpler n-rGO/p-Si Schottky junction solar cells. The n-rGO rather than graphene, which has been successfully developed using NH_3 molecules, is included in the fabrication process of n-rGO/p-Si Schottky junction solar cells. Accordingly, the power conversion efficiency of 9.7 was obtained for prepared devices after applying ammonia treatment for 3 h. For the first time, the developed n-rGO layers are also excellently employed to prepare large n-rGO/p-Si Schottky junction solar cells with ideal *J-V* curves. The improved efficiency of 12.6 % is reached for n-rGO/p-Si Schottky junction solar cells prepared with an active area of 0.6 cm^2. To improve the stability, devices are coated with PMMA as an encapsulated layer, leading to an improvement in the stability for 2 months in the ambient air. Additionally, a recorded efficiency of 13.8 % is achieved. We attribute this development to the chemisorption of ammonia molecules on rGO, which effectively develops the performance of devices.

1. Introduction

The unique properties of graphene have motivated a lot of research interest, leading to employment in different applications since 2004 [1]. One of those applications is as a transparent electrode to extract photo-generated carriers of solar cells [2]. Graphene has been used to prepare graphene/Si Schottky junction solar cells with several structures, which are top-window, top-grid and back-contact [3–6]. The efficiency of prepared devices based on n-Si substrates has significantly increased since 2010. It has also been shown that the graphene area used within the fabrication process is around 0.1 cm^2 to avoid the high density of PMMA residue [6–8] and ensure efficient prepared devices [4,6,9,10]. Techniques such as passivation, forming gas annealing, DUV treatment and chemical doping have been engaged in the preparation of graphene/n-Si Schottky junction solar cells, resulting in an increase in the efficiency of around 16% [6,9]. This indicates that graphene shows an excellent anode electrode for extraction holes. Additionally, it shows that a stable and efficient p-type CVD-graphene is achievable [6,11,12]. In contrast, graphene/p-Si Schottky junction solar devices show low efficiency of about 0.1% [13–15]. The reason for the low efficiency is that there is difficulty in obtaining an effective n-graphene transparent electrode with a suitable doping level and an appropriate interface with p-Si [16,17]. In the reported works for prepared the n-type graphene electrode [18–32], doping processes have been applied to the CVD-graphene surface. However, prepared n-type graphene was inefficient and unstable since graphene is so sensitive to the ambient environment [33]. In addition, it has been reported that applying chemical dopants to transferred CVD-graphene is for reducing the effect of PMMA residue rather than achieving n-doping in transferred graphene [6,34]. Recently, a new approach by using a graphene-heterostructure transparent electrode, which in-

* Corresponding author at: Faculty of Science and Environment Plymouth University, University of Plymouth, Plymouth University, Plymouth PL4 8AA, United Kingdom.
E-mail addresses: ahmed.suhail@plymouth.ac.uk, ahmed.198381@uomosul.edu.iq (A.M. Suhail).

https://doi.org/10.1016/j.cartre.2022.100205

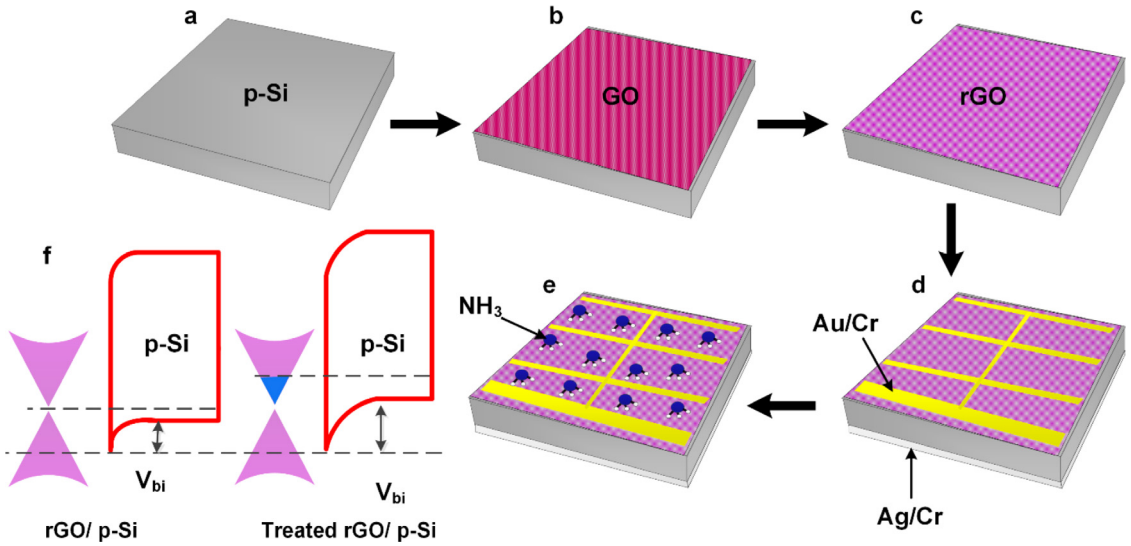

Fig. 1. Preparing process of rGO/p-Si Schottky junction solar cells. (a) Achieving passivation process of p-Si after cleaning and leaving it in ambient air for 2h. (b) Coating GO onto polished- Si substrate. (c) Reducing process of GO by annealing in forming gas. (d) Forming Au/Cr grid and Ag/Cr. (e) Immersing devices in ammonia solution. (f) Developing band structure of rGO/p-Si Schottky junction solar cells after ammonia treatment.

volves oxide-encapsulated layers, chemical treatment and antireflection coating, was used to achieve an efficient graphene-cathode [35–37]. This approach has developed the efficiency to about 12.6% [37]. However, the fabrication process of those devices is complex and expensive. In addition, the deposition process of oxide-encapsulated layers, which were essential to obtain an efficient and stable graphene cathode, requires specific techniques to be achieved since the graphene surface is so sensitive [38–41]. Herein, we introduce a simpler, larger area, lower-cost, more efficient and stable reduced graphene (rGO)/p-Si Schottky solar cell compared with those presented in previous works. The rGO rather than CVD-graphene is used to avoid the PMMA residue obtained from the wet transfer process. The doping process using ammonia solution is effectively employed to increase the n-doping level in rGO. Additionally, the stability of prepared devices has also been investigated and achieved under an ambient environment for 2 months.

2. Experimental section

2.1. Device fabrication

P-type Si substrates with a resistivity of 2-3 Ωcm^{-1} and thickness of 200 µm were used. The RCA procedure was employed to remove the metal ion contaminations. To eliminate the native oxide layer, Si substrates were dipped in a diluted 2% HF solution for 30 s. After that, substrates were exposed to ambient air for 2 hours to naturally achieve the passivation process of Si substrates [41–43]. Graphene oxide solution with a concentration of 0.1 %, which was purchased from Danubia NanoTech (Slovakia), was spin-coated on the polished side of substrates as shown in Fig. 1b. The prepared samples were dried on a hot plate at 150 °C for 15 min. After that, GO samples were annealed in Ar/H_2 at 800 °C for 2 hours to achieve the reduction process. To obtain a low resistance contact to the rGO [43–45], Cr/Au layers were formed as shown in Fig. 1d. Then, Cr/Ag layers were formed on the unpolished side of substrates as shown in the same figure. At that moment, prepared devices were annealed at 550 °C for an hour under a high vacuum to ensure an effective contact at the interfaces of the whole device. To achieve the n doping level in rGO as shown in Figs. 1e and 1 f, the samples were dipped in ammonia solution for various periods in ambient air.

2.2. Device characterization

To investigate the chemical states and atomic ratio of rGO samples before and after the doping process, X-ray photoelectron spectroscopy (XPS) (Kratos AXIS Ultra DLD spectrometer, monochromatic Al Kα emission at 1486.6 eV with an operating power of 150 W) was employed. XPLORA HORIBA system with an Olympus BX41 microscope and green laser source of 532 nm was used to explore Raman spectra of prepared samples. Kysight B1500A Semiconductor Analyser with a solar simulator was used to measure *J-V* curves under AM1.5 conditions with an illumination intensity of 100 mW/cm^2. The calibration process was achieved by using a standard Si solar cell. The external quantum efficiency (EQE) of reduced graphene oxide (rGO)/p-Si Schottky solar cells was measured by using the PVE300 system.

3. Results and discussion

The fabrication process of rGO/p-Si Schottky junction solar cells is presented in Fig. 1. In this work, the rGO rather than CVD-graphene is used to avoid the main problems caused by residual PMMA, which is left on graphene after the wet transfer process [6]. In addition, the top-grid created onto the rGO layer (see Fig. 1d) is crucial since the active area of devices varies between 0.1 and 0.8 cm^2, leading to collection carries from the large area of rGO.

After improving contacts at interfaces using the annealing process, the ammonia treatment was applied to obtain n-rGO as shown in Fig. 1e. This treatment was achieved through immersing rGO/p-Si samples in ammonia solution in the ambient air. The ammonia treatment results in an increase in Fermi levels and built-in voltages at the n-rGO/p-Si junction as displayed in Fig. 1f. The device structure is presented in Fig. 1e. The current density-voltage (*J-V*) characteristics of rGO/p-Si Schottky junction solar cells are displayed in Fig. S3 before and after annealing that was conducted for an hour to ensure an effective contact at the interfaces of the whole device. For an annealed device, the short-circuit current density (J_{SC}), open-circuit voltage (V_{OC}), fill factor (*FF*) and power conversion efficiency (*PCE*) were 21.8 mA/cm^2, 0.4 V, 30% and 2.6%, respectively. For a device that was not annealed, values of photovoltaic parameters were 17 mA/cm^2, 0.4 V, 25% and 1.7%, respectively. It can be observed that there is a clear improvement in the performance of annealed sample compared with that of an un-

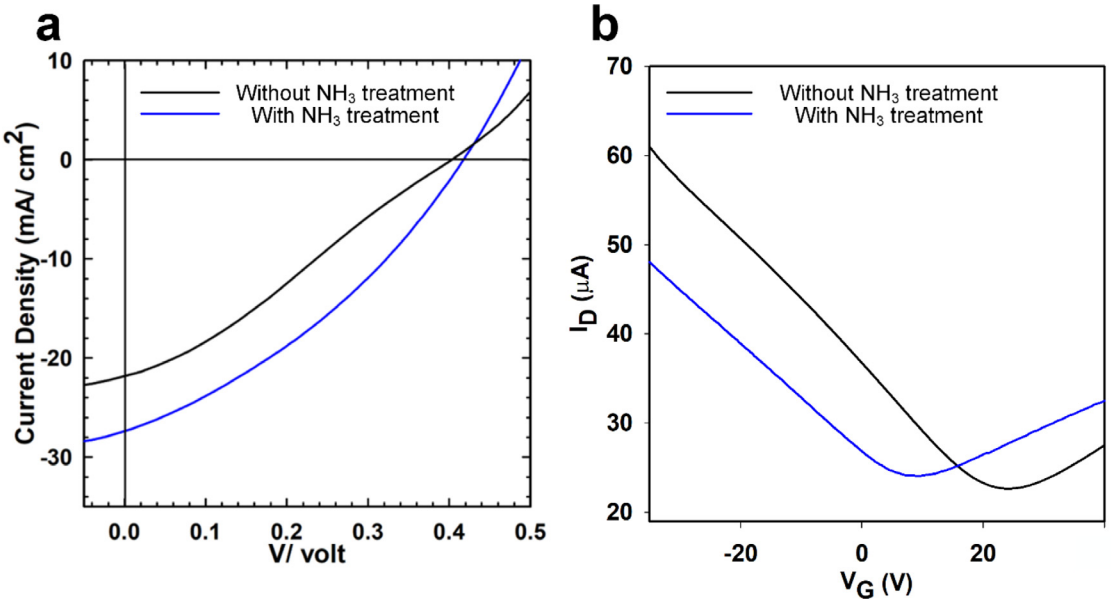

Fig. 2. (a) *J-V* characteristics of reduced graphene oxide (rGO)/p-Si Schottky solar cells with and without ammonia treatment. (b) Current-voltage (I_D-V_G) transfer curves of treated rGO FETs before and after ammonia treatment were measured in air at room temperature and V_D = 0.1 V.

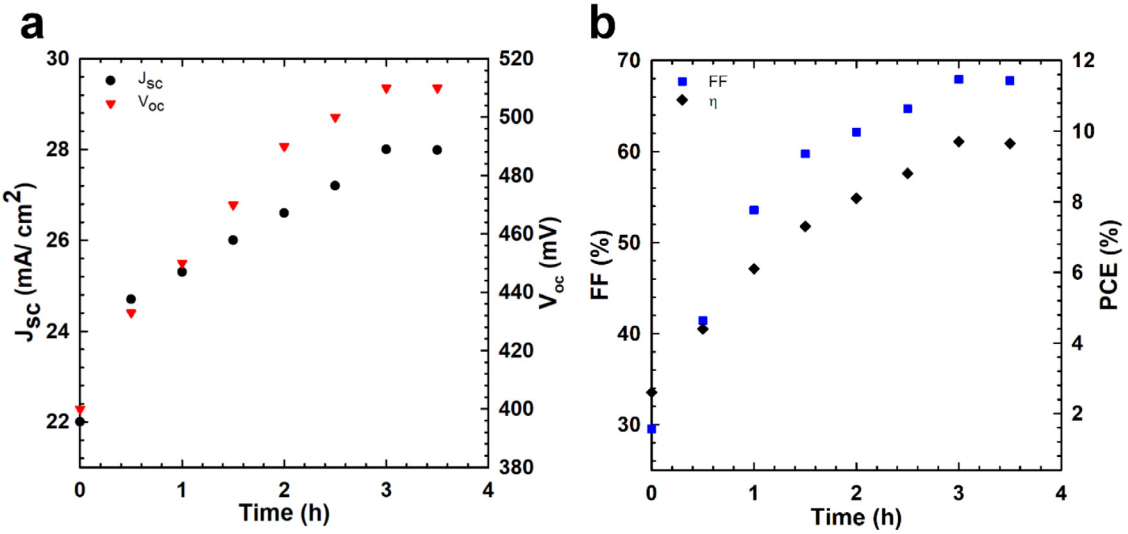

Fig. 3. (a) and (b) Enhancements of V_{OC}, J_{SC}, *FF*, and *PCE* of rGO/p-Si Schottky solar cells treated with ammonia for different periods.

annealed sample. This also shows that the usage of the annealing process is certainly significant for improving the contacts at interfaces, leading to a development in the *PCE* by around 55% in comparison with that of the un-annealed sample. In order to further develop the annealed rGO/p-Si Schottky junction solar cells, samples were immersed in ammonia solution. Fig. 2a compares the *J-V* curves of rGO/p-Si Schottky junction solar cells treated with and without ammonia solution for 30 min. The J_{SC}, V_{OC}, *PCE* and *FF* of the treated device were 24.7 mA/cm^2, 0.43 V, 41% and 4.4%, respectively. This indicates that the *PCE* of treatment of devices is developed by 70% compared with that of the untreated device. To further investigate the doping process, reduced graphene field-effect transistors (RGO-FETs) were also prepared using the methodology reported in our previous work [7]. Fig. 2b shows typical (I_D-V_G) transfer curves of devices before and after ammonia treatment. As observed in this figure, Dirac points of devices were negatively shifted after the treatment. This also shows that the ammonia molecules result in an increase in the n doping level in rGO and a development in solar cell performance. The study of ammonia treatment was systematically explored for a longer time than 30 min to extra investigate the effect of this treatment on the performance of rGO/p-Si Schottky junction solar cells. The average of measured photovoltaic parameters of devices treated for various periods is shown in Figs. 3a and 3b. It can be noticed that the J_{SC} and V_{OC} considerably developed to 28 mA/cm^2 and 0.51 V when the samples were dipped in the ammonia solution for 3 hours. These developments increased the *PCE* to 9.7% and *FF* to 68% Fig. 3b. This indicates that the n-doping level in rGO is successfully achieved via the loading of ammonia molecules onto rGO layers. It can also be observed that photovoltaic parameters of treated samples for longer than 3 hours are mostly saturated, which suggests that the reaction between ammonia and rGO was also saturated and the optimum treatment time is 3 h, which requires to obtain an efficient n-rGO/p-Si Schottky junction solar cells. To discover the nature of development obtained for prepared devices after ammonia treatment, XPS and Raman systems were conducted. The

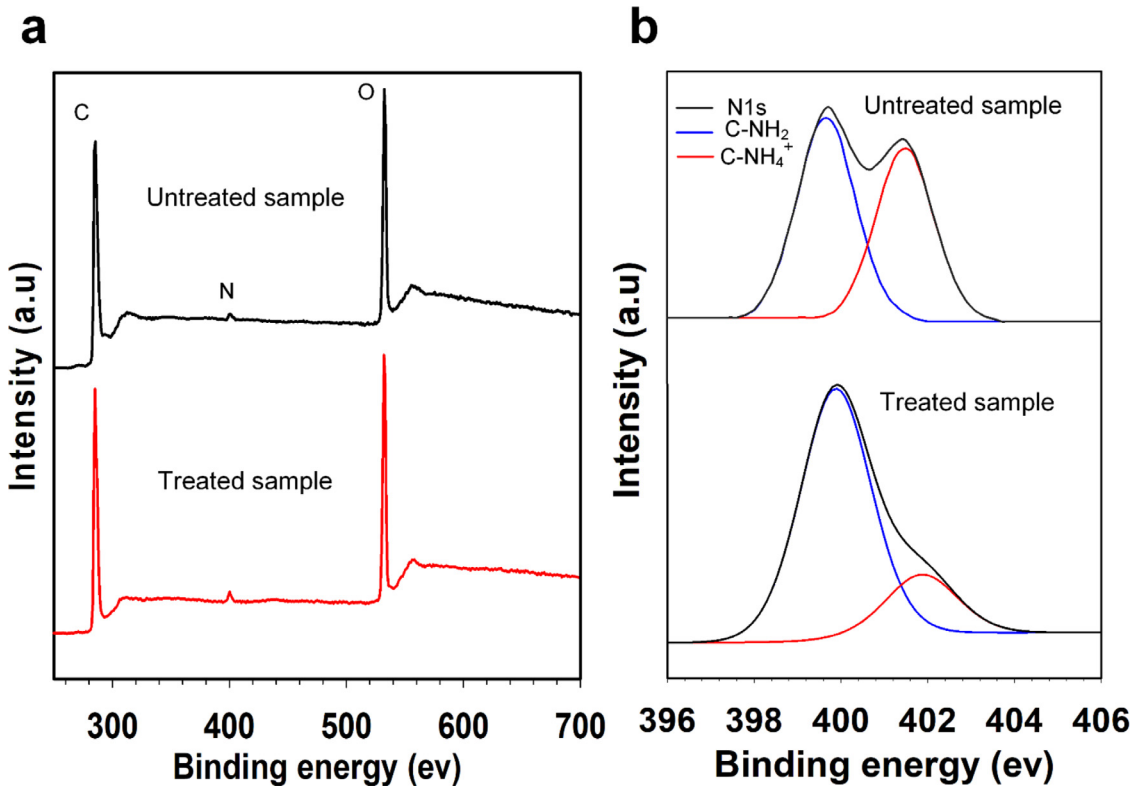

Fig. 4. (a) and (b) survey XPS and N1s results of rGO/p-Si samples treated with and without ammonia for 3 h.

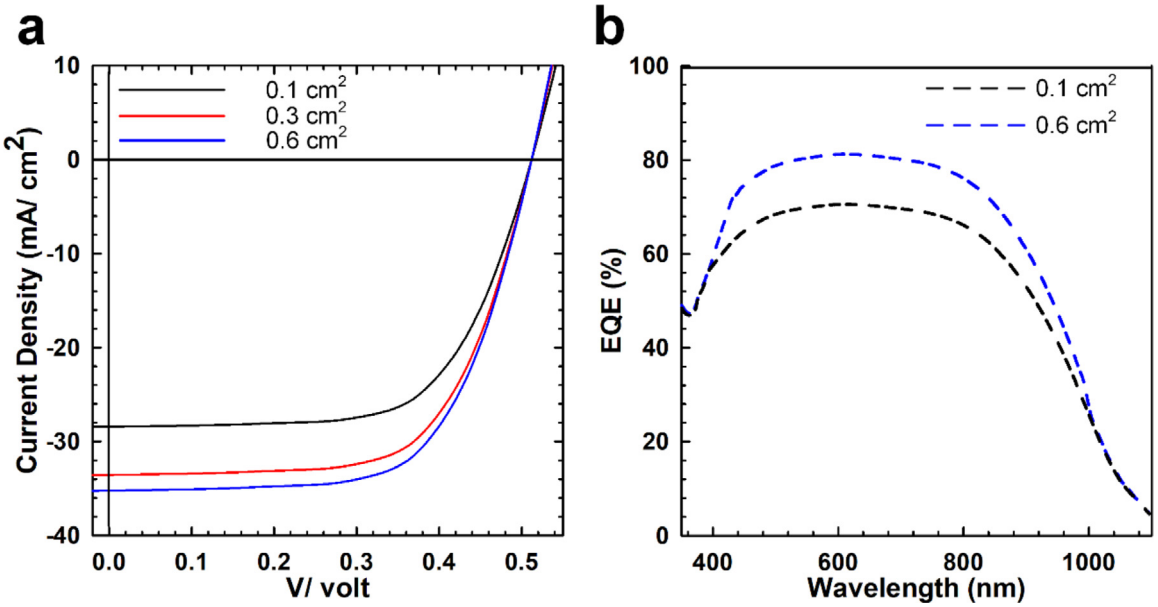

Fig. 5. (a) J-V characteristics of rGO/p-Si Schottky solar cells prepared with various active areas. (b) External quantum efficiency (EQE) spectra of rGO/p-Si Schottky solar cells prepared with 0.1 and 0.6 cm^2 active areas.

data of these measurements are shown in Figs. 4 and S1. Fig. 4a shows the survey XPS spectra of rGO treated before and after the NH_3 treatment for 3 hours.

It can be noticed that the peak of N at around 400 eV increased and the atomic percentage of N developed from 0.7% to 3.2% after the treatment. Where, the presence of a small peak in the spectrum of the untreated sample is from the supplied GO solution. This development in the N component verifies that the NH_3 molecules were loaded onto rGO. To obtain an idea of how these molecules are loaded on the rGO, the N1s high-resolution spectra of rGO samples were measured before and after the treatment. Fig. 4b shows the N1s high-resolution spectra of treated rGO samples with and without NH_3. It can be seen that there are 2 peaks in the spectra of measured samples. The first peak locates at 399.9 eV attributed to C-NH_2. The second peak locates at 401.8 eV, and this belongs to C-NH_4 $^+$. As noticed, the height of the first peak significantly increased after the treatment. In contrast, the height of the second peak was almost the same after the treatment. This veri-

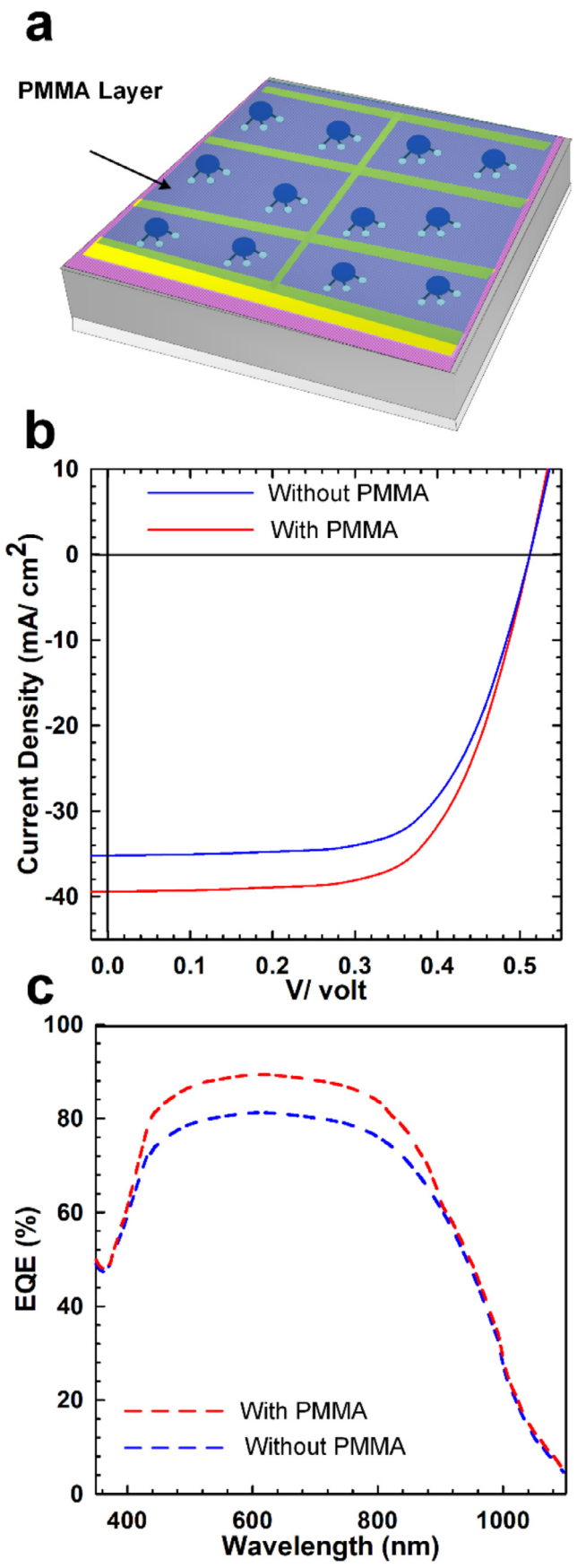

Fig. 6. (a) Schematic of PMMA/n-rGO/p-Si Schottcky junction solar cell. (b) *J-V* characteristics of rGO/p-Si Schottcky junction solar cell coated with and without PMMA layer. (c) External quantum efficiency (EQE) spectra of rGO/p-Si Schottky solar cells coated with and without PMMA layer.

fies that the C-NH_2 component was obtained after the ammonia treatment. This also means that NH_3 molecules are loaded as NH_2 on rGO layers. The mechanism of interacting ammonia molecules as NH_2 occurs in 2 ways. The first way is through the reaction between these molecules and vacancies (or defect sites) in the rGO structure as the rGO is made of flakes stacked together. In this case, the NH_3 interacts and binds with C atoms at those vacancies or defects, forming C-NH_2 bonds. The second way is through the reaction between ammonia and oxygenated functional epoxide groups within rGO. Since the reaction occurs in ambient air, NH_3 molecules attack epoxide groups as a nucleophile, leading to the formation of interacted amino groups within the rGO structure. FTIR data as shown in Fig. S2 also confirms that there is an interaction between NH_3 and rGO through the shifting of peaks at 1042 and 3428 cm^{-1} after the ammonia treatment [46,47]. Hence, it can be said that the reaction between ammonia and rGO occurs via the chemisorption mechanism at room temperature, resulting in an efficient n-doping process and stabilise the structure of rGO. For those devices treated for a longer time than 3 hours, the structure of rGO reaches the stabilized situation and there is no more reaction to be achieved between the molecules and rGO. This is why photovoltaic parameters of rGO/p-Si Schottky junction solar cells treated for prolonged treatment showed no significant development. Fig. S1 shows Raman spectra of treated rGO with and without ammonia for 3 h. After ammonia treatment, the 2D band shifts from 2694 to 2681 cm^{-1}, the G band shifts from 1581 to 1560 cm^{-1}, respectively and the D band shifts from1336 to 1334 cm^{-1}. This shows that there is a red shift in the spectrum of rGO treated with ammonia in comparison with that of the untreated rGO. This also verifies that NH_2 molecules are loaded onto rGO after the treatment. Hence, these molecules will be electron donors to rGO, leading to an improvement in solar cell performance. After optimizing the ammonia treatment for 3 h, devices with a larger active area than 0.1 cm^2 were prepared. Fig. 5 displays the *J-V* characteristics of n-rGO/p-Si solar cell devices prepared with various active areas (0.1, 0.4 and 0.6 cm^2). The J_{SC}, V_{OC}, *FF* and *PCE* of the device prepared with the 0.3 cm^2 active area (red curve) were 33.5 mA/cm^2, 0.51 V, 69% and 11.8%, respectively. For the device prepared with the 0.6 cm^2 (blue curve), the photovoltaic parameters were 35.2 mA/cm^2, 0.51 V, 70% and 12.6%. This indicates that the *PCE* developed by around 30% after increasing the active area of prepared devices from 0.1 to 0.6 cm^2. Our efficiency of 12.6% is the highest efficiency reported so far for n-rGO (or n-graphene)/p-Si Schottky junction solar cells prepared without a capsulation layer [8,18-41]. The idea of increasing the active area was also applied to prepare devices with a larger area than 0.6 cm^2. However, the performance of devices fabricated with a 0.8 cm^2 active area decreases as shown in Table S2. The reason for the lower performance of those devices could be that there is non-uniformity of 0.8 cm^2 area rGO, leading to poor Schottky junction of prepared devices [4]. This also suggests that the optimum active area of n-rGO/p-Si Schottky junction solar cells is 0.6 cm^2. The external quantum efficiency (EQE) spectra were also studied to further verify the development of the performance of n-rGO/p-Si devices prepared with a large active area as shown in Fig. 5b. As observed in this figure, there is a clear significance in the EQE within the visible wavelength region for devices with a larger active area than 0.1 cm^2. It can be seen that the EQE of devices prepared with a 0.6 cm^2 active area increases to about 84% in the wavelength range of 400-950 nm in comparison with that of devices prepared with a 0.1 cm^2 active area. This also shows that the EQE developed by about 30% after increasing the active area from 0.1 to 0.6 cm^2. The developed value of 30% is in an agreement with that based on *J-V* curves, which confirms the development of the performance of devices prepared with large active areas. Even though the *PCE* has greatly been developed after applying the op-

timum ammonia treatment and increasing the active area, the efficiency of prepared devices suffers from a clear degradation after a week. Where the *PCE* reduces from 12.6 to 8.7% as presented in Fig. S6b. The reason for this degradation is that the rGO surface is so sensitive to the ambient environment [6,8,17,34,38-41], leading to reduce the n-doping level. Hence, the PMMA layer was spin-coated on the front side of the device prepared with a 0.6 cm^2 active area as shown in Fig. 6a. Fig. S5 shows the reflectivity of PMMA/n-rGO/p-Si substrates as a function of the wavelength range between 400 and 700 nm. It can be observed that the average diffused reflectance (R) reduced from around 39% to 12%. The *J-V* characteristics of n-rGO/p-Si before and after coating the PMMA layer are shown in Fig. 6b. As presented, for the coated device, the values of J_{SC}, V_{OC}, *FF* and *PCE* were 39 mA/cm^2, 0.51 V, 69% and 13.8%, respectively. This indicates that the *PCE* improved by 12% after reducing the reflected light compared with that of the uncoated device. To the best of our understanding, the *PCE* of 13.8% is a new record for n-rGO/p-Si solar cells reported to date [18,32-41]. Additionally, the coated devices show great stability after storage in the ambient environment for 2 months as shown in Fig. S6a. It can be observed that there is no degradation in the performance of coated devices during the storage time compared with that of uncoated devices (see Fig. S6b). These developments indicate that the benefits of adding the PMMA layer are to reduce the reflected light from the Si surface and improve the stability of prepared devices after ammonia treatment. It is also clear that the fabrication process, which is used in this work for preparing a stable and efficient n-rGO/p-Si Schottky junction solar cell, is simpler than those reported in previous works.

4. Conclusions

A new approach based on the chemisorption of ammonia molecules was introduced to prepare simple, efficient, stable and large n-rGO/p-Si Schottky junction solar cells. It was found that the chemisorption of ammonia plays a vital role in the development of rGO/p-Si Schottky junction solar cell performance. This technique improved the *PCE* to 9.7% after immersing samples in ammonia solution for 3 h. Additionally, rGO/p-Si Schottky junction solar cells with large active areas and ideal *J-V* curves were efficiently prepared for the first time after including the optimum ammonia treatment, resulting in an improvement in the efficiency to 12.6%. The stability of prepared devices was also developed by coating PMMA as an encapsulated layer. The coated devices showed great stability for 2 months in the ambient environment with no degradation in the value of *PCE*. The usage of coated layer also results in a decrease in the reflectivity of Si substrates. These developments improve the efficiency of prepared devices to13.8 %. It can be concluded that the introduced work is an effective and crucial way to fabricate low-cost, simple, stable and high-performance n-rGO/p-Si Schottky junction solar cells.

Declaration of Competing Interest

The authors declare that they have no known competing financial interests or personal relationships that could have appeared to influence the work reported in this paper.

Acknowledgment

We acknowledge the financial support from the University of Plymouth under EU Horizon 2020 MSCA-ITN-ETN AiPBAND (grant number 764281) and the technical assistant of Mina Safarzadeh. The authors would also like to thank the University of Mosul (https://www.uomosul.edu.iq/en/) / Mosul, Iraq for its support to complete this work.

Supplementary materials

Supplementary material associated with this article can be found, in the online version, at doi:10.1016/j.cartre.2022.100205.

References

[1] K.S. Novoselov, et al., A roadmap for graphene, Nature 490 (7419) (2012) 192–200.
[2] Y. Lin, et al., Graphene/semiconductor heterojunction solar cells with modulated antireflection and graphene work function, Energy Environ. Sci. 6 (1) (2013) 108–115.
[3] A. Di Bartolomeo, Graphene Schottky diodes: An experimental review of the rectifying graphene/semiconductor heterojunction, Phys. Rep. 606 (2016) 1–58.
[4] Y. Wang, et al., Top-grid monolayer graphene/Si Schottkey solar cell, J. Solid State Chem. 224 (2015) 102–106.
[5] Y. Ye, L. Dai, Graphene-based Schottky junction solar cells, J. Mater. Chem. 22 (46) (2012) 24224–24229.
[6] A. Suhail, et al., Improved efficiency of graphene/Si Schottky junction solar cell based on back contact structure and DUV treatment, Carbon 129 (2018) 520–526.
[7] A. Suhail, et al., Reduction of polymer residue on wet–transferred CVD graphene surface by deep UV exposure, Appl. Phys. Lett. 110 (18) (2017) 183103.
[8] A.M. Suhail, Graphene/silicon Schottky Junction Solar Cells with High Efficiency, University of Plymouth, 2019.
[9] Y. Song, et al., Role of interfacial oxide in high-efficiency graphene–silicon Schottky barrier solar cells, Nano Lett. 15 (3) (2015) 2104–2110.
[10] A. Suhail, et al., Effective chemical treatment for high efficiency graphene/si schottky junction solar cells with a graphene back-contact structure, Adv. Mater. Lett. 8 (10) (2017) 977–982.
[11] H. Park, et al., Interface engineering of graphene for universal applications as both anode and cathode in organic photovoltaics, Sci. Rep. 3 (1) (2013) 1–8.
[12] D. Zhang, et al., Al-TiO2 composite-modified single-layer graphene as an efficient transparent cathode for organic solar cells, ACS nano 7 (2) (2013) 1740–1747.
[13] S.K. Behura, et al., Junction characteristics of chemically-derived graphene/p-Si heterojunction solar cell, Carbon 67 (2014) 766–774.
[14] M. Mohammed, et al., Junction investigation of graphene/silicon Schottky diodes, Nanoscale Res. Lett. 7 (1) (2012) 1–6.
[15] C. Xie, et al., Monolayer graphene film/silicon nanowire array Schottky junction solar cells, Appl. Phys. Lett. 99 (13) (2011) 133113.
[16] G. Luongo, et al., Electronic properties of graphene/p-silicon Schottky junction, J. Phys. D Appl. Phys. 51 (25) (2018) 255305.
[17] F. Schedin, et al., Detection of individual gas molecules adsorbed on graphene, Nat. Mater. 6 (9) (2007) 652–655.
[18] S. Srivastava, et al., Nitrogen doped high quality CVD grown graphene as a fast responding NO 2 gas sensor, New J. Chem. 42 (12) (2018) 9550–9556.
[19] A. Di Bartolomeo, et al., Graphene–silicon schottky diodes for photodetection, IEEE Trans. Nanotechnol. 17 (6) (2018) 1133–1137.
[20] S.M. Shinde, et al., Grain structures of nitrogen-doped graphene synthesized by solid source-based chemical vapor deposition, Carbon 96 (2016) 448–453.
[21] F. Zhang, et al., Molecular-reductant-induced control of a graphene–organic interface for electron injection, Chem. Mater. 31 (17) (2019) 6624–6632.
[22] M.F. Khan, et al., Stable and reversible doping of graphene by using KNO 3 solution and photo-desorption current response, RSC Adv. 5 (62) (2015) 50040–50046.
[23] J. Baltazar, et al., Photochemical doping and tuning of the work function and dirac point in graphene using photoacid and photobase generators, Adv. Funct. Mater. 24 (32) (2014) 5147–5156.
[24] H. Gao, et al., Synthesis of S-doped graphene by liquid precursor, Nanotechnology 23 (27) (2012) 275605.
[25] K.C. Kwon, et al., Work-function decrease of graphene sheet using alkali metal carbonates, J. Phys. Chem. C 116 (50) (2012) 26586–26591.
[26] R. Lv, et al., Large-area Si-doped graphene: controllable synthesis and enhanced molecular sensing, Adv. Mater. 26 (45) (2014) 7593–7599.
[27] B. Guo, et al., Controllable N-doping of graphene, Nano Lett. 10 (12) (2010) 4975–4980.
[28] P. Wei, et al., Tuning the Dirac point in CVD-grown graphene through solution processed n-type doping with 2-(2-methoxyphenyl)-1, 3-dimethyl-2, 3-dihydro-1 H-benzoimidazole, Nano Lett. 13 (5) (2013) 1890–1897.
[29] M. Ovezmyradov, et al., Chemical vapor deposition of phosphorous-and boron–doped graphene using phenyl-containing molecules, J. Nanosci. Nanotechnol. 15 (7) (2015) 4883–4886.
[30] C. Zhang, et al., CVD synthesis of nitrogen-doped graphene using urea, Sci. China: Phys. Mech. Astron. 58 (10) (2015) 1–6.
[31] R. Lv, et al., Nitrogen-doped graphene: beyond single substitution and enhanced molecular sensing, Sci. Rep. 2 (1) (2012) 1–8.
[32] X. Shi, et al., Selective n-type doping in graphene via the aluminium nanoparticle decoration approach, J. Mater. Chem. C 2 (27) (2014) 5417–5421.
[33] E. Shi, et al., Colloidal antireflection coating improves graphene–silicon solar cells, Nano Lett. 13 (4) (2013) 1776–1781.
[34] J.W. Suk, et al., Enhancement of the electrical properties of graphene grown by chemical vapor deposition via controlling the effects of polymer residue, Nano Lett. 13 (4) (2013) 1462–1467.

[35] P.-H. Ho, et al., Sunlight-activated graphene-heterostructure transparent cathodes: enabling high-performance n-graphene/p-Si Schottky junction photovoltaics, Energy Environ. Sci. 8 (7) (2015) 2085–2092.
[36] K. Cui, S. Maruyama, Multifunctional graphene and carbon nanotube films for planar heterojunction solar cells, Prog. Energy Combust. Sci. 70 (2019) 1–21.
[37] S. Yavuz, et al., Enhanced environmental stability coupled with a 12.5% power conversion efficiency in an aluminum oxide-encapsulated n-graphene/p-silicon solar cell, ACS Appl. Mater. Interfaces 10 (43) (2018) 37181–37187.
[38] K. Nagashio, A. Toriumi, Density-of-states limited contact resistance in graphene field-effect transistors, Japan. J. Appl. Phys. 50 (7R) (2011) 070108.
[39] B. Dlubak, et al., Are Al 2 O 3 and MgO tunnel barriers suitable for spin injection in graphene? Appl. Phys. Lett. 97 (9) (2010) 092502.
[40] M.H. Maneshian, et al., The influence of high dielectric constant aluminum oxide sputter deposition on the structure and properties of multilayer epitaxial graphene, Nanotechnology 22 (20) (2011) 205703.
[41] M. Friedemann, et al., Versatile sputtering technology for Al2O3 gate insulators on graphene, Sci. Technol. Adv. Mater. (2012).
[42] A.G. Aberle, Surface passivation of crystalline silicon solar cells: a review, Prog. Photovoltaics Res. Appl. 8 (5) (2000) 473–487.
[43] B.-S. Wu, et al., Hybrid multi-layer graphene/Si Schottky junction solar cells, in: 2013 IEEE 39th Photovoltaic Specialists Conference (PVSC), IEEE, 2013.
[44] Y. Xu, et al., Contacts between two-and three-dimensional materials: ohmic, Schottky, and p–n heterojunctions, ACS Nano 10 (5) (2016) 4895–4919.
[45] X. Miao, et al., High efficiency graphene solar cells by chemical doping, Nano Lett. 12 (6) (2012) 2745–2750.
[46] S. Kang, et al., Interfacial polymerized reduced graphene oxide covalently grafted polyaniline nanocomposites for high-performance electromagnetic wave absorber, J. Mater. Sci. 54 (8) (2019) 6410–6424.
[47] J. Zhang, et al., N-substituted carboxyl polyaniline covalent grafting reduced graphene oxide nanocomposites and its application in supercapacitor, Electrochim. Acta 199 (2016) 70–79.